Chemical Science

EDGE ARTICLE

View Article Online
View Journal | View Issue

Cite this: *Chem. Sci.*, 2019, **10**, 5766

All publication charges for this article have been paid for by the Royal Society of Chemistry

An oxygen self-sufficient NIR-responsive nanosystem for enhanced PDT and chemotherapy against hypoxic tumors†

Guoliang Yang,‡[a] Jia Tian,‡[a] Chao Chen,[b] Dawei Jiang,[a] Yudong Xue,[a] Chaochao Wang,[a] Yun Gao[a] and Weian Zhang*[a]

Received 26th February 2019
Accepted 22nd April 2019

DOI: 10.1039/c9sc00985j

rsc.li/chemical-science

The efficacy of photodynamic therapy and chemotherapy is largely limited by oxygen deficiency in the hypoxic tumor microenvironment. To solve these problems, we fabricated a novel NIR-responsive nanosystem which could co-deliver oxygen and anticancer drug DOX. An oxygen self-sufficient amphiphile (F-IR780-PEG) was first synthesized and subsequently utilized to load anticancer drug DOX to form nanoparticles (F/DOX nanoparticles). Due to the high oxygen capacity of such nanoparticles, the hypoxic tumor microenvironment was greatly modulated after these nanoparticles reached the tumor region, and the results revealed that hypoxia-inducible factor α (HIF-1α) was down-regulated and the expression of P-glycoprotein (P-gp) was then reduced, which were in favor of chemotherapy. Under light irradiation at 808 nm, IR780 could efficiently produce singlet oxygen to damage cancer cells by photodynamic therapy (PDT). Simultaneously, the IR780 linkage could be cleaved by singlet oxygen generated by itself and resulted in DOX release, which further caused cell damage by chemotherapy. With the combination of PDT and chemotherapy, F/DOX nanoparticles showed remarkable therapeutic efficacy under *in vitro* and *in vivo* conditions. Furthermore, the F/DOX nanoparticles are favorable for imaging-guided tumor therapy due to the inherent fluorescence properties of IR780. We thus believe that the synergistic treatment described here leads to an ideal therapeutic approach to hypoxic tumors.

Introduction

Tumor hypoxia, which originates from distorted tumor vasculatures and irregular cancer cell proliferation,[1] is a great challenge for overcoming resistance to cancer therapies, especially for photodynamic therapy (PDT)[2] and chemotherapy.[3] As far as PDT employs a light-excited photosensitizer (PS) to generate cytotoxic singlet oxygen ($^1O_2$) by consuming tumor-dissolved oxygen (O_2) for cancer treatment,[4] the PDT efficiency is largely limited by inadequate oxygen in tumors. In addition, cancer cells will activate hypoxia-inducible factor α (HIF-1α) in a hypoxia environment,[5] and then increase the expression of P-glycoprotein (P-gp),[6] which as a membrane efflux pump transports chemotherapeutic drugs out of cells to cause hypoxia-induced drug resistance.[7] In recent years, various strategies have already been developed to modulate tumor hypoxia for improving the efficacy of PDT, such as transporting oxygen into tumor by using artificial blood substitutes (*e.g.*, perfluorocarbons),[8] promoting intratumor blood flow[9] as well as producing oxygen inside the tumors by catalysts.[10] Liu and his coworkers improved the PDT effect by using MnO_2 to modulate the hypoxic tumor microenvironment by *in situ* generating O_2 through the reaction with tumor endogenous H_2O_2.[11] Meanwhile, several studies have demonstrated that reversing hypoxia in tumors would enhance the chemotherapy effect.[3,12] Cai *et al.* developed oxygen-nanocarriers where hemoglobin (Hb) and DOX were encapsulated within the cancer cell membrane to overcome hypoxia-induced chemoresistance.[12]

Recently, many studies on tumor treatments have been focused on combined therapies with the cooperative enhancement interactions between two or more treatments to produce superadditive therapeutic effects.[13] It has been proved that PDT has the potential to enhance chemotherapy efficacy since ROS generation from PDT is able to promote intracellular drug delivery and accelerate drug release, increasing the cytotoxicity of anticancer drugs.[14] To date, numerous studies have been designed to realize synergistic therapeutic effects of chemo-photodynamic therapy by loading anticancer drugs and photosensitizers together into nanoassemblies, obtaining a higher therapeutic effect.[15] For example, Zhang *et al.* fabricated a multifunctional prodrug where the singlet oxygen could be

[a]*Shanghai Key Laboratory of Functional Materials Chemistry, Key Laboratory for Specially Functional Polymeric Materials and Related Technology of the Ministry of Education, East China University of Science and Technology, 130 Meilong Road, Shanghai 200237, China. E-mail: wazhang@ecust.edu.cn*

[b]*State Key Laboratory of Bioreactor Engineering Center, East China University of Science and Technology, China*

† Electronic supplementary information (ESI) available. See DOI: 10.1039/c9sc00985j

‡ These authors contributed equally to this work.

generated from TPP under irradiation and then anticancer drug gemcitabine was released after the thioketal linkage was cleaved, obtaining significant tumor synergistic therapeutic efficacy.[16] Yin and her co-workers designed a phototheranostic nanodrug (PTN), which generated $^1O_2$ and accelerated the release of anticancer drug camptothecin (CPT) into cancer cells upon red light irradiation, showing enhanced performance for cancer theranostics.[17] Despite holding great promise, most studies for chemo-photodynamic synergistic therapy are not for hypoxic tumors where these treatments are weakened, which makes these treatments inefficient for cancer therapy. Although some studies have involved the synergistic treatment between PDT and chemotherapy in hypoxic tumors,[18] it is still a significant challenge to enhance the therapeutic efficiency of these two therapies in hypoxic tumors at the same time.

Herein, to achieve a high efficiency of synergistic treatments between PDT and chemotherapy in hypoxic tumors, we constructed a smart nanocarrier by using an amphiphile, F-IR780-PEG (Scheme 1), which could not only modulate the tumor hypoxia microenvironment by employing perfluorocarbon as an oxygen carrier, but could also enhance the release efficiency of encapsulated DOX in a controllable manner. In this system, IR780 plays two important roles: *i.e.* as a NIR photosensitizer[19] and a light-triggered degradable[20] linker between the hydrophobic perfluorocarbon and hydrophilic PEG chain. IR780 is susceptible to photobleaching through a photooxidative cleavage reaction, and the photooxidation pathway of these molecules entails $^1O_2$-mediated cleavage of the polyene *via* dioxetane intermediates. Anti-cancer drug DOX was encapsulated by F-IR780-PEG to form F-IR780-PEG/DOX (F/DOX) nanoparticles, and the toxicity of DOX greatly decreased by taking advantage of the encapsulation of nanoparticles.[21] F/DOX nanoparticles could accumulate efficiently in the tumor after intravenous injection (i.v.) due to the enhanced permeability and retention (EPR) effect.[22] After F/DOX nanoparticles enter the tumor hypoxic region, oxygen carried by perfluorocarbons will be released to relieve tumor hypoxia, where HIF-1α is down-regulated and then the expression of P-gp is reduced (Scheme 1b). Under 808 nm laser irradiation, F/DOX nanoparticles could produce ROS abundantly because of the adequate supply of oxygen, which performs a highly efficient PDT. Moreover, the encapsulated DOX is quickly released during the PDT process, as the linker, IR780, is degraded with illumination, which induces the disassembly of F/DOX nanoparticles. It is worthy of note that released DOX would mostly stay inside cells owing to the decreased expression of P-gp, which could achieve effective chemotherapy. A series of experiments including *in vitro* and *in vivo* experiments have been performed to verify our above assumptions. Our work demonstrates that F/DOX nanoparticles can be used as efficient agents for enhancing the anti-cancer effect of PDT and chemotherapy synergistic therapy in hypoxic tumors.

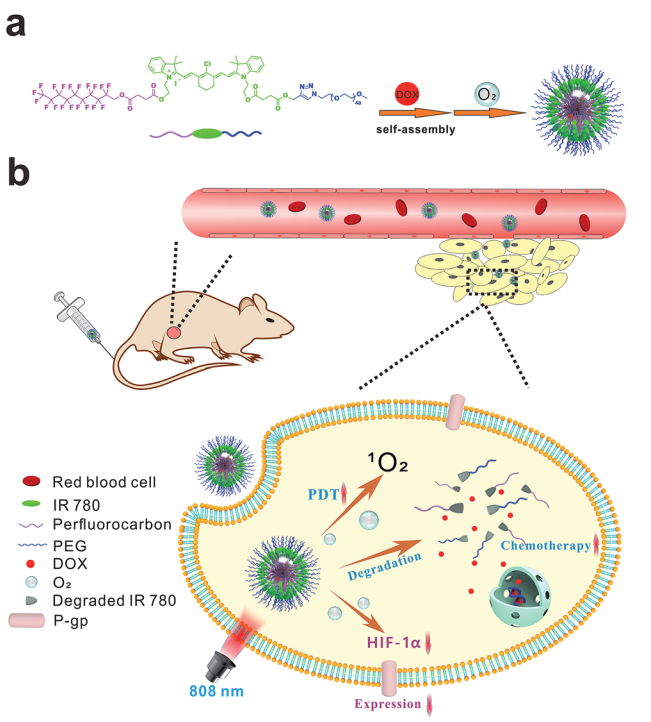

Scheme 1 Schematic illustration for the fabrication of F/DOX nanoparticles (a), and the processes of enhanced tumor therapy of photodynamic therapy and chemotherapy in tumor tissue (b).

Results and discussion

Synthesis, preparation and characterization of F/DOX NPs

To construct a smart nanocarrier for improving the high efficiency of synergistic treatments between PDT and chemotherapy, the amphiphile, F-IR780-PEG, was prepared and the detailed synthetic procedures are depicted in Scheme S1.† IR780 was firstly synthesized according to the previous literature with some changes.[23] To functionalize IR780, propargyl alcohol and heptadecafluoro-1-nonanol were reacted separately with succinic anhydride in anhydrous THF to produce compounds **4** and **6**. The ^{19}F NMR spectrum of compound **4** exhibits a single peak at −80.83 ppm, which is assigned to trifluoromethyl (Fig. S5†). The peaks of H_2 and H_3 at 2.66 ppm demonstrate that compound **4** was successfully synthesized (Fig. S4†). IR780 was first reacted with compound **4** to produce asymmetric IR780 through an esterification reaction, and then asymmetric IR780 was further reacted with compound **6** through the same synthetic approach to obtain F-IR780-alkynyl (**7**). In the ^{1}H NMR spectrum of compound **7**, the peaks of H_6 (from 6.33 to 6.36 ppm) and H_7 (from 8.28 to 8.31 ppm) are ascribed to heptamethylene chain protons of IR780 (Fig. S8†). Four different peaks for heptamethylene chain protons (H_6, H_7, H_{11} and H_{12}) of compound **6** (Fig. S7†) turned into two peaks (H_6 and H_7) of compound **7**, indicating that perfluorocarbon was covalently conjugated to IR780. This was also confirmed by the mass spectrum of compound **7**, where a peak appears at m/z 1213.31 corresponding to $[\text{F-IR780-alkynyl} - \text{I}]^+$ (Fig. S9†). Finally, amphiphilic F-IR780-PEG (**9**) was prepared *via* a typical 'click' reaction between F-IR780-alkynyl and azido-PEG. In the ^{1}H NMR spectrum of compound **9**, the peak of H_3 at 7.73 ppm corresponding to 1,2,3-triazole demonstrates that PEG was conjugated

successfully to compound 7 (Fig. S10†). In addition, amphiphilic C-IR780-PEG as a control was synthesized by using docosanoic acid through a similar strategy, and the detailed synthetic procedure is given in Scheme S2.† Chemical structures were characterized by ^{1}H NMR, ^{19}F NMR and mass spectroscopy (MS), and the spectra are presented in Fig. S1–S13.†

Amphiphilic F-IR780-PEG and C-IR780-PEG could self-assemble into micelles through a dialysis method,[24] and the obtained micelles were denoted as F micelles and C micelles, respectively. Next, the anticancer drug DOX was encapsulated into F micelles through hydrophobic interaction to form F-IR780-PEG/DOX (F/DOX) nanoparticles, respectively. As shown in Fig. 1a, F-IR780-PEG in DMF showed characteristic absorbance of IR780 in the near-infrared region, but its F micelles had a broad absorbance of IR780 with a strong shoulder peak due to the formation of H-aggregation of IR780 in the micelles.[25] For F/DOX nanoparticles, although a similar absorbance spectrum was found with F micelles in the NIR region, the weak absorbance at 490 nm could still be distinguished, indicating that DOX was entrapped in micelles successfully. Additionally, C micelles had a similar UV-Vis absorbance spectrum to F micelles (Fig. S14†). The drug-loading efficiency (DL) and entrapment efficiency (EE) of F/DOX nanoparticles were 6.4% and 15.6% respectively, which were determined by the UV-Vis method. The average diameter of F micelles and F/DOX nanoparticles measured with dynamic light scattering was 122 nm and 138 nm, respectively (Fig. 1b), which were similar to the size of nanoparticles observed by transmission electron microscopy (TEM) (Fig. 1d and e). Meanwhile, the micelles retained good stability during fifteen days with no obvious change in particle size (Fig. 1c). However, the size distribution of F/DOX nanoparticles obviously changed after laser irradiation, and the corresponding morphology change was also observed by TEM (Fig. 1f), suggesting that the nanoparticles were disrupted with laser irradiation.

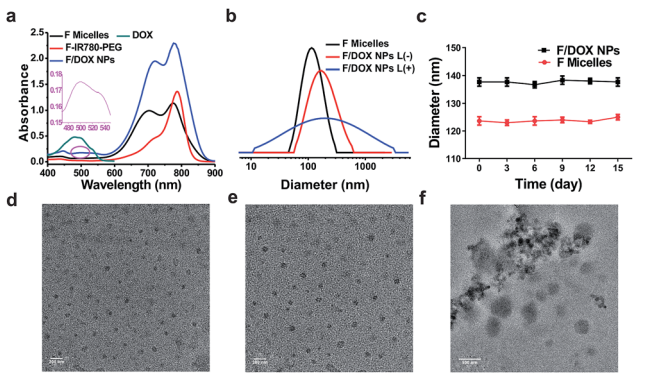

Fig. 1 Characterization of micelles. (a) UV-Vis absorption spectra of F/DOX nanoparticles, F micelles, DOX in PBS (pH = 7.4), and F-IR780-PEG in DMF. (b) Size distributions of F/DOX nanoparticles before and after laser irradiation and F micelles in PBS (pH = 7.4). (c) The physical stability of F micelles and F/DOX nanoparticles in PBS (pH = 7.4). Each data point was expressed as mean ± standard deviation (n = 3). TEM images of (d) F micelles, (e) F/DOX nanoparticles before laser irradiation, and (f) F/DOX nanoparticles after laser irradiation.

Singlet oxygen generation and drug release behavior

To confirm the oxygen-carrying ability of F micelles and F/DOX nanoparticles, we tested dissolved oxygen of different samples by using a dissolved oxygen detector, with PBS as the control. It was observed that the values of dissolved oxygen in PBS and C micellar solution were 8.23 and 8.31, respectively. In contrast, the values of F micelles and F/DOX nanoparticles were 16.79 and 16.93, respectively (Fig. 2a). The values of dissolved oxygen of solutions containing a perfluorocarbon analog (F micelles and F/DOX nanoparticles) were more than two fold the values of solutions without the perfluorocarbon analog (PBS and C micelles), which meant that F micelles and F/DOX nanoparticles had an oxygen-carrying capacity. As IR780 is a typical photosensitizer[19] and $^{1}O_2$ will be generated by light irradiation, the ability for $^{1}O_2$ generation was measured by detecting the absorbance of 1,3-diphenylisobenzofuran (DPBF), and the absorbance decrease of DPBF in the presence of $^{1}O_2$ corresponds to the production of $^{1}O_2$. We recorded the changes of absorbance of DPBF in the presence of C micelles, F micelles and F/DOX nanoparticles with 808 nm laser irradiation for 10 s intervals (Fig. S15†). Although the absorbance of DPBF decreased in the presence of all these samples with laser, the decrease rate was obviously different, indicating that they had different single oxygen quantum yields. The absorbance of DPBF at 425 nm with different irradiation times is shown in Fig. 2b; the rate of absorbance decrease in the presence of F micelles was similar to that of F/DOX nanoparticles, which was almost 3 fold faster than that in the presence of C micelles. The phenomenon indicated that the single oxygen quantum yield of F micelles or F/DOX nanoparticles was higher than that of C micelles, which was caused by the higher amount of oxygen carried by the perfluorocarbon.

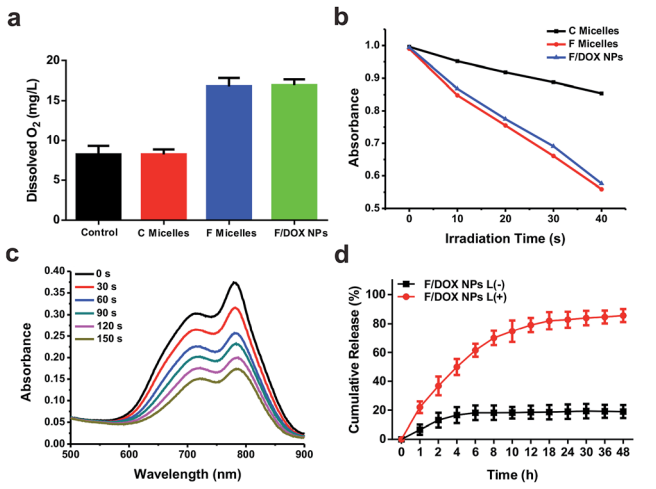

Fig. 2 (a) Dissolved O_2 of different micelles or nanoparticles with PBS as the control. Each data point was expressed as mean ± standard deviation (n = 3). (b) Plots of the change in absorption at 425 nm of DPBF solutions with C micelles, F micelles and F/DOX nanoparticles added upon irradiation at 808 nm. (c) UV-Vis absorption spectra of F/DOX nanoparticles with different 808 nm laser irradiation times. (d) *In vitro* DOX release profiles from F/DOX nanoparticles with and without laser irradiation in PBS at pH = 7.4. Each data point was expressed as mean ± standard deviation (n = 3).

Photo-bleaching is a typical feature of IR780 because it is sensitive to ROS produced by itself with light exposure, and the ROS will attack and break the heptamethine chain of IR780 to degrade IR780.[20] We then measured the degradation of IR780 inside F/DOX nanoparticles under different laser irradiation times through an UV-Vis detector. The absorbance of IR780 inside F/DOX decreased with illumination time (Fig. 2c), indicating that IR780 can be degraded under light exposure. We also measured the degradation rate of IR780 in F micelles and C micelles. As shown in Fig. S16,† the IR780 degradation rate in F micelles was faster than in C micelles, which confirmed that more $^1O_2$ was generated by F micelles from another side. As IR780 acted as a linker between the hydrophobic perfluorocarbon moiety and hydrophilic PEG chain, the nanoparticles could be decomposed when IR780 was photo-bleached with laser irradiation. Additionally, we assumed that the loaded-DOX would be released when nanoparticles were disrupted with laser irradiation. To verify this speculation, the light-triggered DOX release was quantitatively evaluated after F/DOX nanoparticles were illuminated with an 808 nm laser. As shown in Fig. 2d, approximately 20% of loaded-DOX was released both from F/DOX nanoparticles at 48 h without laser irradiation, revealing that nanoparticles were quite stable. However, it was surprising to find that nearly 80% of loaded-DOX was released from F/DOX nanoparticles with laser irradiation. This phenomenon indicated that the loaded-DOX could be released effectively from F/DOX nanoparticles as we expected.

In vitro anti-tumor treatment and mechanism

To evaluate the cell uptake of nanoparticles, MCF-7 cells incubated with C micelles, F micelles and F/DOX nanoparticles for different times were investigated by confocal laser scanning microscopy (CLSM) (Fig. 3a). It can be observed that the fluorescence of IR780 inside cells for all samples was enhanced with incubation time increasing, indicating that more and more micelles or nanoparticles were internalized by MCF-7 cells. Meanwhile, quantitative intracellular uptake of DOX from F/DOX nanoparticles for different incubation times was also tested by flow cytometry (Fig. 3b), and the fluorescence intensity of DOX inside cells was remarkably enhanced with incubation time, which was similar to the result of IR780 from CLSM. After these different nanoparticles could be well taken up by cells, the cell behavior was then investigated under hypoxic conditions by detecting expressions of HIF-1α and P-gp. MCF-7 cells were incubated under hypoxia conditions with C micelles, F micelles, and F/DOX nanoparticles, with PBS as a control. HIF-1α expressions were firstly measured by Western blot analysis (Fig. 3c). Apparent accumulation of HIF-1α was detected in hypoxia MCF-7 cells when treated with PBS and C micelles, while low expressions of HIF-1α occurred in cells after treatment with F micelles and F/DOX nanoparticles. Therefore, it was demonstrated that HIF-1α down-regulated observably when hypoxic MCF-7 cells were treated with F micelles and F/DOX nanoparticles, indicating that the expression of HIF-1α was modulated with oxygen carried by F micelles and F/DOX nanoparticles. Furthermore, expressions of P-gp were analyzed

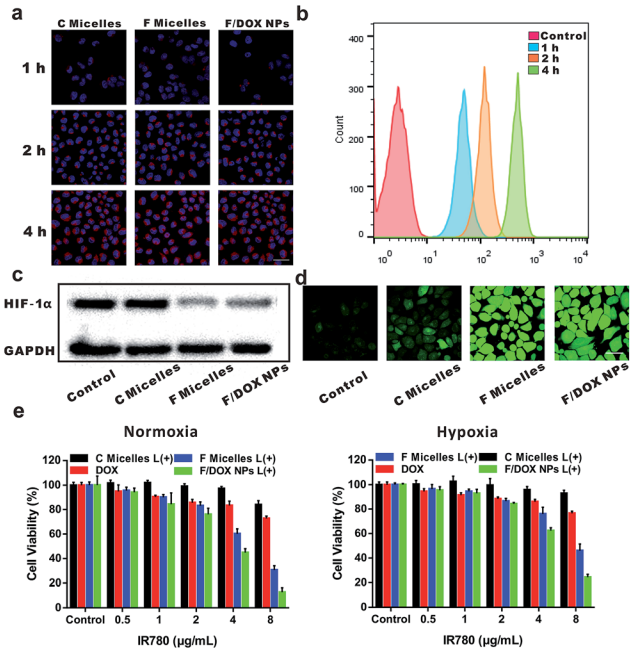

Fig. 3 (a) MCF-7 cell uptake of C micelles, F micelles and F/DOX nanoparticles at different times (1, 2, and 4 h). The scale bar represents 50 μm. (b) Flow cytometry analysis of DOX fluorescence in MCF-7 cells incubated with F/DOX nanoparticles for 1, 2 and 4 h. (c) HIF-1α expressions of MCF-7 cells treated with C micelles, F micelles and F/DOX nanoparticles under hypoxia conditions. (d) CLSM images of intracellular ROS generation with laser irradiation in MCF-7 cells. The scale bar represents 50 μm. (e) Cell viability of MCF-7 cells treated with free DOX, C micelles, F micelles or F/DOX nanoparticles with 808 nm laser irradiation under normoxic and hypoxic conditions. Data are given as the mean ± SD ($n = 5$).

by confocal microscopy (Fig. S17†). High expressions of P-gp in MCF-7 cells treated with C micelles under hypoxia conditions were observed. In contrast, P-gp expressions decreased to a rather low level after treatment with F micelles and F/DOX nanoparticles, which were consistent with the results of HIF-1α expressions (Fig. 3c). These results indicated that oxygen-containing samples (F micelles and F/DOX nanoparticles) could greatly suppress HIF-1α expressions and further inhibit P-gp expressions under hypoxia conditions, suggesting that the O_2 carried by these nanoparticles endowed them with the ability to overcome hypoxia-induced chemoresistance. Intracellular ROS generation in MCF-7 cells was further investigated by the ROS probe 2′,7′-dichlorodihydrofluorescein diacetate (DCFH-DA). As shown in Fig. 3d, after laser irradiation, there was negligible fluorescence in the PBS treatment group but cells treated with other samples showed clearly green fluorescence, indicating that ROS was generated within cells treated with micelles or nanoparticles after laser irradiation. Moreover, green fluorescence intensities in cells treated with F micelles or F/DOX nanoparticles were much stronger than that of C micelles, demonstrating that more ROS was produced by perfluorocarbon-containing micelles or nanoparticles, which was consistent with the above results obtained using DPBF as the detector (Fig. 2b). Intracellular DOX release with laser

irradiation was also evaluated by confocal microscopy (Fig. S18†). In the absence of 808 nm laser irradiation, it was distinctly found that the red fluorescent IR780 nearly merged with the green fluorescence of DOX, which confirmed that the F/DOX nanoparticles mostly remained in the cytoplasm of MCF-7 cells. However, after laser irradiation, the majority of DOX fluorescence separated from the IR780 fluorescence, implying the disassembly of F/DOX nanoparticles with illumination. Furthermore, it was found that the green fluorescence of DOX was in good agreement with the blue fluorescence of the nuclei staining with DAPI, suggesting that DOX was almost completely released and moved into the nucleus. Therefore, it could be concluded that the release of DOX encapsulated in F/DOX nanoparticles can be well controlled with laser irradiation.

Based on the above results, it is reasonable to propose that F/DOX nanoparticles could be beneficial in terms of enhancing the cancer cell-killing efficacy under both normoxia and hypoxia conditions. Therefore, the anti-tumor efficacy of F/DOX nanoparticles and other contrast formulations against MCF-7 cells was evaluated. The biocompatibilities of C micelles, F micelles and F/DOX nanoparticles were firstly studied (Fig. S19†), and we can find that the viabilities of cells were all above 80% whenever under normoxic or hypoxic conditions, indicating that these samples all had good biocompatibility. Next, the cell viabilities of MCF-7 cells were evaluated to determine the efficiency of PDT, chemotherapy and synergistic therapy. As shown in Fig. 3e, there was only slight inhibition in free DOX treatment. Compared with cells treated with free DOX under normoxic conditions, viabilities of MCF-7 cells under hypoxic conditions were slightly higher, which was caused by hypoxia-induced chemoresistance. The PDT efficiency was then determined by examining the cell viability of MCF-7 cells. Under 808 nm laser irradiation, the PDT efficiency of F micelles was obviously higher than that of C micelles at different concentrations under both normoxic and hypoxic conditions, due to a greater number of ROS produced by F micelles, which was agreeable with that measured by DPBF and CLSM. Here, cell death caused by the photothermal effect of IR780 could be ignored with laser irradiation for 30 s, since there was only a slight temperature increase under short irradiation time (Fig. S20a†).[8,26] Subsequently, we compared the synergistic efficacy with the single therapeutic efficacy of PDT and chemotherapy. As we expected, the synergistic treatment using F/DOX nanoparticles with laser irradiation showed the most effective cancer cell killing under both normoxia and hypoxia conditions. Therefore, F/DOX nanoparticles as an O_2-self-sufficient agent could improve PDT efficiency and enhanced chemotherapeutic efficacy.

In vivo tumor imaging and anti-tumor effects

Encouraged by the good anticancer efficacy of F/DOX nanoparticles under 808 nm laser *in vitro*, we then carried out animal experiments to evaluate their therapeutic potency. The *in vivo* distributions of F/DOX nanoparticles at different times were first determined *via* a small animal imaging system (Fig. 4a). It was clearly observed that the IR780 fluorescence signal of F/DOX nanoparticles gradually increased in the tumor region

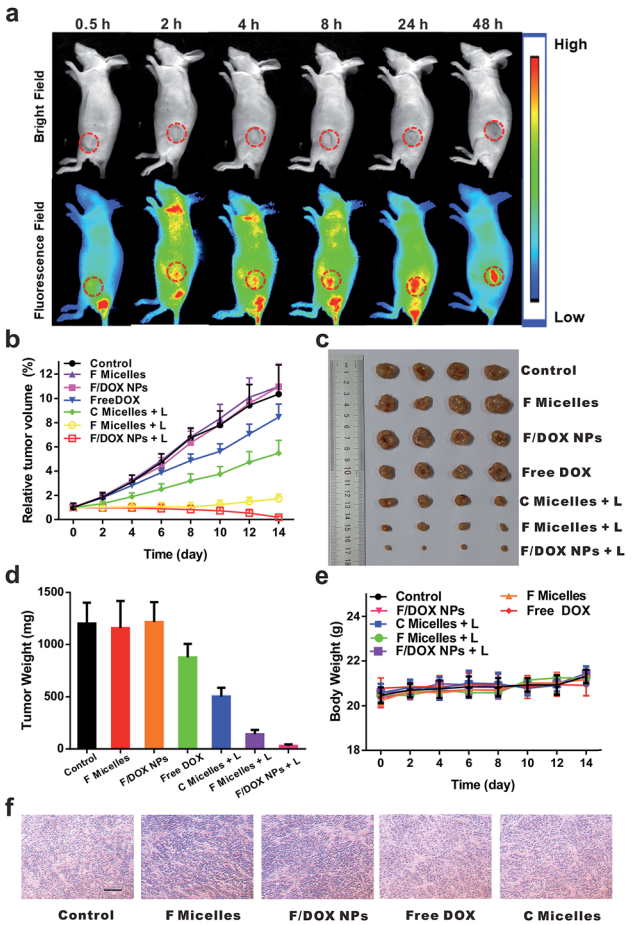

Fig. 4 (a) Fluorescence images of MCF-7 tumor-bearing mice post i.v. injection of F/DOX nanoparticles for different times. (b) Tumor growth curves of tumor-bearing nude mice after various treatments. (c) Photographs of excised tumors from representative mice after various treatments. (d) Tumor weights measured after various treatments. (e) Body weight changes of tumor-bearing nude mice after various treatments. (f) Immunohistochemical staining of HIF-1α protein in tumor tissue in various treatment groups. The scale bar represents 100 μm.

after intravenous administration due to the EPR effect. After 48 h, the mice were sacrificed and the tumor and organs were harvested for imaging (Fig. S21†). Obviously, the IR780 fluorescence signal in the tumor was stronger than that in other normal organs, which confirmed F/DOX nanoparticles could effectively accumulate and strand in tumors.

To investigate the antitumor efficiency of F/DOX nanoparticles *in vivo*, MCF-7 tumor-bearing nude model mice were intravenously administered saline, F micelles with laser (F micelles + L), or without laser, F/DOX nanoparticles with laser (F/DOX NPs + L) or without laser, C micelles with laser (C micelles + L) and free DOX, respectively. Under the guidance of *in vivo* imaging, the tumor tissue was irradiated with an 808 nm laser at 48 h post-injection. The tumor volume was monitored every other day over the following 14 days. To avoid the photothermal effect during the treatment, we divided the irradiation time into two consecutive 30 s applications with a 1 min

interval in between (Fig. S20b†). As shown in Fig. 4b and c, the treatment with free DOX showed just slight tumor growth inhibition (which may be attributed to the insufficient quantity of drugs and hypoxia-induced drug resistance) compared with other groups of saline, F micelles and F/DOX nanoparticles. The treatment with F micelles with 808 nm laser irradiation showed significant tumor growth inhibition which was much higher than that of the treatment with C micelles, which was attributed to more oxygen carried by F micelles. Therefore, the PDT efficacy could be well enhanced by transporting oxygen into the tumor hypoxia region. In contrast, the treatment with F/DOX nanoparticles with laser irradiation resulted in the highest anti-tumor efficacy, which confirmed the superiority of synergistic photodynamic therapy and light-triggered chemotherapy. In addition, the average tumor weight of different treatments in Fig. 4d also indicated that the F/DOX NPs + L group exhibited the most efficient anticancer effect. Collectively, these results demonstrated that F/DOX nanoparticles under laser irradiation could obviously overcome the problems of drug resistance and low efficiency of photodynamic therapy caused by tumor hypoxia. Additionally, the body weight of mice was recorded every other day and there was no notable change during the period of treatment (Fig. 4e).

Meanwhile, the antitumor efficacy was further checked by the immunohistochemical studies of tumor slices after the treatments (Fig. S22†). All of the saline, unilluminated F micelles and F/DOX nanoparticle groups demonstrated compact tumor cells. Meanwhile, the free DOX treatment group presented only slight inhibition to tumor growth, which is in line with the tumor growth curve shown in Fig. 4b. Also, mild tumor cell necrosis can be observed in the illuminated C micelle group. However, there was intensive tumor cell necrosis in the group of F micelles under laser irradiation, which was attributed to more oxygen carried by F micelles. As expected, tumor cells revealed the highest level of tumor cell damage in the treatment group of F/DOX nanoparticles with illumination, certifying that the best anti-tumor efficacy could be achieved under the synergistic effect of enhanced PDT and chemotherapy. The degree of tumor hypoxia of different groups was also measured, and the expression of HIF-1α *in vivo* was tested by immunohistochemical analysis (Fig. 4f). Notably, the expressions of HIF-1α of F micelle and F/DOX nanoparticle treatment groups were obviously smaller compared with other groups, and obvious down-regulation of HIF-1α was also observed for these two perfluorocarbon-containing samples. These results demonstrated that oxygen carried in these nanoparticles could efficiently suppress the activation of HIF-1α and reduce tumor hypoxia. Therefore, F/DOX nanoparticles could present the possibility to enhance the PDT and overcome hypoxia-induced drug resistance. The systemic toxicity was further analyzed by histological analysis of the major organs, performed with H&E staining (Fig. S22†). There were no detectable physiological morphology changes in the major organs, such as the liver, heart, spleen, lung, and kidney in all treatment groups, which corresponded to results of body weight of mice. These results demonstrated the good biocompatibility of our nanoparticles and their promising prospects for *in vivo* application.

Conclusions

In this work, we successfully fabricated a light-triggered drug release nanoplatform of F/DOX nanoparticles to enhance the efficiency of synergistic treatments between PDT and chemotherapy in hypoxic tumors. Such F/DOX nanoparticles delivered anti-cancer drug DOX and oxygen to tumors with DOX controlled release by light. F/DOX nanoparticles accumulated efficiently in the tumor after intravenous injection (i.v.). Benefiting from the oxygen self-supply ability, the hypoxia microenvironment of tumors was greatly altered, which is not only helpful for enhancing the efficacy of oxygen-dependent PDT but also for overcoming hypoxia-induced chemoresistance by inhibition of the HIF-1α induced P-gp expression. The anti-tumor effect of F/DOX nanoparticles has been achieved in cells and tumor-bearing mice, and *in vitro* and *in vivo* results evidenced the advantages of F/DOX nanoparticles in killing tumor cells and destroying solid tumors. Therefore, this work supplies a novel strategy for the fabrication of nanocarriers to combat tumor hypoxia induced chemoresistance and inefficient PDT.

Conflicts of interest

There are no conflicts to declare.

Acknowledgements

This work was financially supported by the National Natural Science Foundation of China (No. 21574039 and 51803058) and Shanghai Sailing Program (No. 19YF1410900). All animal procedures were performed in accordance with Chinese legislation on the Use and Care of Research Animals (Document No. 55, 2001), and institutional guidelines for the Care and Use of Laboratory Animals established by the East China University of Science and Technology Animal Studies Committee, and this committee approved the experiments.

Notes and references

1 W. R. Wilson and M. P. Hay, *Nat. Rev. Cancer*, 2011, **11**, 393–410.

2 X. Li, N. Kwon, T. Guo, Z. Liu and J. Yoon, *Angew. Chem., Int. Ed.*, 2018, **57**, 11522–11531; Z. Lv, H. Wei, Q. Li, X. Su, S. Liu, K. Y. Zhang, W. Lv, Q. Zhao, X. Li and W. Huang, *Chem. Sci.*, 2018, **9**, 502–512; D. Zhang, Z. Cai, N. Liao, S. Lan, M. Wu, H. Sun, Z. Wei, J. Li and X. Liu, *Chem. Sci.*, 2018, **9**, 7390–7399; S. Kolemen, T. Ozdemir, D. Lee, G. M. Kim, T. Karatas, J. Yoon and E. U. Akkaya, *Angew. Chem., Int. Ed.*, 2016, **55**, 3606–3610.

3 F. Li, H. Mei, Y. Gao, X. Xie, H. Nie, T. Li, H. Zhang and L. Jia, *Biomaterials*, 2017, **145**, 56–71; D. Samanta, D. M. Gilkes, P. Chaturvedi, L. Xiang and G. L. Semenza, *Proc. Natl. Acad. Sci. U. S. A.*, 2014, **111**, E5429–E5438; J. Yang, W. Li,

L. Luo, M. Jiang, C. Zhu, B. Qin, H. Yin, X. Yuan, X. Yin, J. Zhang, Z. Luo, Y. Du and J. You, *Biomaterials*, 2018, **182**, 145–156.

4 W. Fan, P. Huang and X. Chen, *Chem. Soc. Rev.*, 2016, **45**, 6488–6519; X. Li, S. Yu, Y. Lee, T. Guo, N. Kwon, D. Lee, S. C. Yeom, Y. Cho, G. Kim, J.-D. Huang, S. Choi, K. T. Nam and J. Yoon, *J. Am. Chem. Soc.*, 2019, **141**, 1366–1372; N. Alifu, X. Dong, D. Li, X. Sun, A. Zebibula, D. Zhang, G. Zhang and J. Qian, *Mater. Chem. Front.*, 2017, **1**, 1746–1753; C. Gui, E. Zhao, R. T. K. Kwok, A. C. S. Leung, J. W. Y. Lam, M. Jiang, H. Deng, Y. Cai, W. Zhang, H. Su and B. Z. Tang, *Chem. Sci.*, 2017, **8**, 1822–1830; M. Chen, W. Xie, D. Li, A. Zebibula, Y. Wang, J. Qian, A. Qin and B. Z. Tang, *Chem.–Eur. J.*, 2018, **24**, 16603–16608; X. Chen, D. Lee, S. Yu, G. Kim, S. Lee, Y. Cho, H. Jeong, K. T. Nam and J. Yoon, *Biomaterials*, 2017, **122**, 130–140.

5 D. M. Gilkes, G. L. Semenza and D. Wirtz, *Nat. Rev. Cancer*, 2014, **14**, 430–439; S. Dawar, N. Singh, R. K. Kanwar, R. L. Kennedy, R. N. Veedu, S.-F. Zhou, S. Krishnakumar, S. Hazra, S. Sasidharan, W. Duan and J. R. Kanwar, *Drug Discovery Today*, 2013, **18**, 1292–1300.

6 K. M. Comerford, T. J. Wallace, J. Karhausen, N. A. Louis, M. C. Montalto and S. P. Colgan, *Cancer Res.*, 2002, **62**, 3387–3394.

7 J. Abraham, N. N. Salama and A. K. Azab, *Leuk. Lymphoma*, 2015, **56**, 26–33.

8 R. Song, D. Hu, H. Y. Chung, Z. Sheng and S. Yao, *ACS Appl. Mater. Interfaces*, 2018, **10**, 36805–36813; Y. Cheng, H. Cheng, C. Jiang, X. Qiu, K. Wang, W. Huan, A. Yuan, J. Wu and Y. Hu, *Nat. Commun.*, 2015, **6**, 8785.

9 H. Gong, Y. Chao, J. Xiang, X. Han, G. Song, L. Feng, J. Liu, G. Yang, Q. Chen and Z. Liu, *Nano Lett.*, 2016, **16**, 2512–2521.

10 Y. Liu, Y. Jiang, M. Zhang, Z. Tang, M. He and W. Bu, *Acc. Chem. Res.*, 2018, **51**, 2502–2511.

11 T. Gu, L. Cheng, F. Gong, J. Xu, X. Li, G. Han and Z. Liu, *ACS Appl. Mater. Interfaces*, 2018, **10**, 15494–15503.

12 H. Tian, Z. Luo, L. Liu, M. Zheng, Z. Chen, A. Ma, R. Liang, Z. Han, C. Lu and L. Cai, *Adv. Funct. Mater.*, 2017, **27**, 1703197.

13 D. Luo, K. A. Carter, D. Miranda and J. F. Lovell, *Adv. Sci.*, 2017, **4**, 1600106; W. Fan, B. Yung, P. Huang and X. Chen, *Chem. Rev.*, 2017, **117**, 13566–13638; T.-T. Zhang, C.-H. Xu, W. Zhao, Y. Gu, X.-L. Li, J.-J. Xu and H.-Y. Chen, *Chem. Sci.*, 2018, **9**, 6749–6757; J.-C. Yang, Y. Shang, Y.-H. Li, Y. Cui and X.-B. Yin, *Chem. Sci.*, 2018, **9**, 7210–7217.

14 C.-Y. Sun, Z. Cao, X.-J. Zhang, R. Sun, C.-S. Yu and X. Yang, *Theranostics*, 2018, **8**, 2939–2953.

15 H.-W. Liu, X.-X. Hu, K. Li, Y. Liu, Q. Rong, L. Zhu, L. Yuan, F.-L. Qu, X.-B. Zhang and W. Tan, *Chem. Sci.*, 2017, **8**, 7689–7695; R. Liang, S. You, L. Ma, C. Li, R. Tian, M. Wei, D. Yan, M. Yin, W. Yang, D. G. Evans and X. Duan, *Chem. Sci.*, 2015, **6**, 5511–5518.

16 L.-H. Liu, W.-X. Qiu, B. Li, C. Zhang, L.-F. Sun, S.-S. Wan, L. Rong and X.-Z. Zhang, *Adv. Funct. Mater.*, 2016, **26**, 6257–6269.

17 C. Ji, Q. Gao, X. Dong, W. Yin, Z. Gu, Z. Gan, Y. Zhao and M. Yin, *Angew. Chem., Int. Ed.*, 2018, **57**, 11384–11388.

18 S. Xu, X. Zhu, C. Zhang, W. Huang, Y. Zhou and D. Yan, *Nat. Commun.*, 2018, **9**, 2053; L. Feng, L. Cheng, Z. Dong, D. Tao, T. E. Barnhart, W. Cai, M. Chen and Z. Liu, *ACS Nano*, 2017, **11**, 927–937.

19 G. Liu, S. Zhang, Y. Shi, X. Huang, Y. Tang, P. Chen, W. Si, W. Huang and X. Dong, *Adv. Funct. Mater.*, 2018, **28**, 1804317; L. Tan, J. Li, X. Liu, Z. Cui, X. Yang, S. Zhu, Z. Li, X. Yuan, Y. Zheng, K. W. K. Yeung, H. Pan, X. Wang and S. Wu, *Adv. Mater.*, 2018, **30**, 1801808; S. Ma, J. Zhou, Y. Zhang, B. Yang, Y. He, C. Tian, X. Xu and Z. Gu, *ACS Appl. Mater. Interfaces*, 2019, **11**, 7731–7742; C. Zhao, Y. Tong, X. Li, L. Shao, L. Chen, J. Lu, X. Deng, X. Wang and Y. Wu, *Small*, 2018, **14**, 1703045.

20 K. Mitra, C. E. Lyons and M. C. T. Hartman, *Angew. Chem., Int. Ed.*, 2018, **57**, 10263–10267; R. R. Nani, A. P. Gorka, T. Nagaya, T. Yamamoto, J. Ivanic, H. Kobayashi and M. J. Schnermann, *ACS Cent. Sci.*, 2017, **3**, 329–337; R. R. Nani, J. A. Kelley, J. Ivanic and M. J. Schnermann, *Chem. Sci.*, 2015, **6**, 6556–6563; A. P. Gorka and M. J. Schnermann, *Curr. Opin. Chem. Biol.*, 2016, **33**, 117–125.

21 Y. Zhu, J. Zhang, F. Meng, C. Deng, R. Cheng, J. Feijen and Z. Zhong, *J. Controlled Release*, 2016, **233**, 29–38; W. Chen, S. Yang, F. Li, C. Qu, Y. Liu, Y. Wang, D. Wang and X. Zhang, *Acta Biomater.*, 2018, **81**, 219–230; J. Chen, J. Ding, Y. Wang, J. Cheng, S. Ji, X. Zhuang and X. Chen, *Adv. Mater.*, 2017, **29**, 1701170.

22 Y. Cai, P. Liang, Q. Tang, X. Yang, W. Si, W. Huang, Q. Zhang and X. Dong, *ACS Nano*, 2017, **11**, 1054–1063; J. L. Perry, K. G. Reuter, J. C. Luft, C. V. Pecot, W. Zamboni and J. M. DeSimone, *Nano Lett.*, 2017, **17**, 2879–2886; R. Liu, W. Xiao, C. Hu, R. Xie and H. Gao, *J. Controlled Release*, 2018, **278**, 127–139; C. Yan, Z. Guo, Y. Shen, Y. Chen, H. Tian and W.-H. Zhu, *Chem. Sci.*, 2018, **9**, 4959–4969.

23 A. P. Thomas, L. Palanikumar, M. T. Jeena, K. Kim and J.-H. Ryu, *Chem. Sci.*, 2017, **8**, 8351–8356; Q. Lv, X. Yang, M. Wang, J. Yang, Z. Qin, Q. Kan, H. Zhang, Y. Wang, D. Wang and Z. He, *J. Controlled Release*, 2018, **279**, 234–242; S. Luo, X. Tan, S. Fang, Y. Wang, T. Liu, X. Wang, Y. Yuan, H. Sun, Q. Qi and C. Shi, *Adv. Funct. Mater.*, 2016, **26**, 2826–2835; S.-Y. Lim, K.-H. Hong, D. I. Kim, H. Kwon and H.-J. Kim, *J. Am. Chem. Soc.*, 2014, **136**, 7018–7025.

24 J. Wang, Y. Liu, Y. Ma, C. Sun, W. Tao, Y. Wang, X. Yang and J. Wang, *Adv. Funct. Mater.*, 2016, **26**, 7516–7525; M.-P. Chien, M. P. Thompson, E. C. Lin and N. C. Gianneschi, *Chem. Sci.*, 2012, **3**, 2690–2694.

25 L. Qin, F. Xie, X. Jin and M. Liu, *Chem.–Eur. J.*, 2015, **21**, 11300–11305; K. Pal, V. Sharma, D. Sahoo, N. Kapuria and A. L. Koner, *Chem. Commun.*, 2018, **54**, 523–526; F. Nicoli, M. K. Roos, E. A. Hemmig, M. Di Antonio, R. de Vivie-Riedle and T. Liedl, *J. Phys. Chem. A*, 2016, **120**, 9941–9947; J. Li, B. Lv, D. Yan, S. Yan, M. Wei and M. Yin, *Adv. Funct. Mater.*, 2015, **25**, 7442–7449.

26 H. Ren, J. Liu, F. Su, S. Ge, A. Yuan, W. Dai, J. Wu and Y. Hu, *ACS Appl. Mater. Interfaces*, 2017, **9**, 3463–3473.

